(Received 24 June 2025, Accepted 20 August 2025, Scheduled 31 August 2025)

Compact Multi-Port Millimeter-Wave MIMO Antenna with 360° Radiation Coverage

Jingchang Nan, Licong Fan*, Shuming Liu, and Yifei Wang

School of Electronics and Information Engineering, Liaoning University of Engineering and Technology, Huludao, China

ABSTRACT: In order to meet antenna requirements for vehicular communication, a compact multiport MIMO antenna design is proposed for the n261 frequency band in 5G millimeter-wave communication. The 3D size of the antenna is $16 \times 16 \times 17\,\text{mm}^3$. By optimizing the radiation patches and layout, a four-port MIMO antenna is developed, with adjacent antenna elements positioned on both sides of the dielectric substrate to minimize coupling between antenna units. Additionally, optimization is performed to achieve 360° radiation coverage for the multiport MIMO antenna. The simulation and measurement results show that the proposed antenna covers the n261 frequency band with an operational bandwidth. The overall isolation between ports of the multiport MIMO antenna is also relatively high. The 12-port MIMO antenna operates in the frequency range of 27.28 to 28.67 GHz, with a gain of 6.25 dBi, and its radiation pattern demonstrates diversity, providing complete 360 ° coverage in both elevation and azimuth planes. Therefore, the proposed antenna not only has a compact size and simple structure but also supports radiation propagation across multiple planes, reducing multipath propagation losses and enhancing communication quality and reliability. It satisfies the requirements of vehicular communication for 5G millimeter wave MIMO antennas.

1. INTRODUCTION

With the rapid development of autonomous driving and vehicle-to-everything (V2X) technologies, the demand for communication bandwidth to support vehicle sensor fusion and real-time environmental perception exceeds gigabits per second. The traditional Sub-6 GHz frequency band, due to spectrum resource depletion, can no longer meet this critical demand. The millimeter-wave frequency band, with its abundant continuous spectrum resources, has become the core technological solution to support high-capacity vehicle communication for 5G and future 6G. Among them, the n261 band (27.5–28.35 GHz), due to its relatively low atmospheric attenuation (< 0.2 dB/km) and global spectrum availability, has been explicitly defined by the 3GPP standard as a key deployment band for vehicular communication [1–4]. However, deploying millimeter-wave communication in the dynamic and complex vehicular environment with the n261 band presents extremely stringent and specific requirements for antenna design. The antenna must effectively cover the entire bandwidth of the n261 band, 850 MHz, to support high-throughput V2X data exchange, such as real-time HD map updates and multi-sensor data sharing. Additionally, to cope with the high-speed movement of vehicles, complex posture changes such as turning or pitching, and signal obstructions caused by vehicle metallic structures like A-pillar and hood, the antenna must have wide-angle coverage capabilities, typically requiring a beam coverage of at least $\pm 60°$ or even omnidirectional 360° coverage to ensure continuity and robustness of the communication link. Furthermore, due to the strict constraints of installation space, such as rear view mirrors and bumpers, the antenna structure must meet miniaturization requirements. Finally, to mitigate the Doppler shift caused by high-speed motion, overcome multipath fading, and improve channel capacity and reliability, the antenna must support a multi-port high-isolation design. The isolation between ports should exceed 15 dB to enable efficient spatial diversity and multiplexing, which is critical for ensuring high-reliability, low-latency communication between vehicles and between vehicles and infrastructure in the future [5–8].

In recent years, the research on vehicular multiple-input multiple-output (MIMO) antennas supporting 5G millimeter-wave communication has continued to deepen, with recent advancements in diversity gain and isolation improvement. Ref. [9] proposes a decoupled MIMO antenna with a radiation pattern in the E-plane, achieving multi-directional radiation through a multifunctional dielectric decoupler. However, its beam direction is fixed, making it difficult to adapt to changes in vehicular posture. The filtering MIMO antenna in [10] utilizes substrate integrated waveguide (SIW) orthogonal modes for spatial diversity, but it cannot adjust the coverage angle. The five-port MIMO antenna in [11] combines patch antennas with dipoles to achieve polarization/direction pattern diversity, but its size reaches $1.03\lambda_0 \times 1.03\lambda_0$, which will expand to $146\,\text{mm}^2$ at the 28 GHz band, far exceeding the limitations of vehicular installation space. Similarly, although the ultra-wideband unit design in [12] achieves a 6 GHz bandwidth, its 8×8 array size is difficult to integrate into rear view mirrors or bumpers. The dual-band MIMO antenna in [13] uses a metal-wire metamaterial wall to improve isolation by 36 dB but introduces additional resonant structures. The reconfigurable MED antenna in [14] integrates three-port functionality but relies on

* Corresponding author: Licong Fan (a401214916@163.com).

parasitic strips and narrow slots, increasing process complexity. None of the above solutions address the core needs of vehicular scenarios, which are to achieve 360° beam coverage, high isolation, and compact size through a simple physical structure [15–24].

This paper proposes the design of a multi-port MIMO antenna with 360° radiation coverage, suitable for vehicular communication. The basic antenna unit is a simple patch antenna, with the radiating patch shaped like a "question mark". The antenna units are arranged perpendicularly at 90° to each other, forming a 2×2 four-port MIMO antenna. The adjacent units are positioned on the upper and lower sides of the dielectric to reduce antenna coupling. The substrate size is only $15 \times 15 \times 0.254\,\text{mm}^3$. Based on this design, by rotating the four-port MIMO antenna, 2×4 eight-port and 3×4 twelve-port MIMO antennas are constructed. The antenna gain reaches 6.25 dBi, and without adding complex decoupling structures, the isolation between antenna ports exceeds 18 dB. Additionally, the antenna achieves multi-dimensional mode diversity, meeting the requirements for vehicular communication.

2. DESIGN OF ANTENNA

2.1. Design of Monopole Antenna

The minimum unit size of the antenna proposed in this paper is $6 \times 5 \times 0.254\,\text{mm}^3$, with the dielectric material being Rogers 5880, having a dielectric constant of 2.2. The antenna uses a 50 Ω microstrip line feeding mechanism. According to transmission line theory, the width of the radiating patch of a rectangular microstrip antenna can be estimated using Equation (1):

$$w = \frac{c}{2f}\sqrt{\frac{2}{\epsilon_r + 1}} \tag{1}$$

In the formula: c is the speed of light, f the resonant center frequency, and ϵ_r the dielectric constant of the material. A short-circuited line is added to the rectangular microstrip antenna to design a bent monopole antenna resonating at 28 GHz. The total length is estimated using Equation (2):

$$L = W_e = \lambda_{28\,\text{GHz}}/4 \tag{2}$$

The optimization process of the metal radiating patch on the antenna is shown in Fig. 1. With the antenna's design, the variation of the reflection coefficient S_{11}, gain, and the radiation pattern of the unit are illustrated in Fig. 2. The final form of the antenna exhibits dual-resonance characteristics, which is due to the initial patch design resonating at 20 GHz. After adding a stub, the antenna forms a curved folded monopole, generating additional resonance in the millimeter-wave frequency band. By extending the current flow path, the antenna's radiation characteristics are improved. The antenna's radiation pattern shows omnidirectionality in the E-plane and a dumbbell shape in the H-plane, conforming to the radiation pattern of a monopole antenna, indicating the antenna's stability. The subsequent research in this paper focuses on the millimeter-wave frequency band of the antenna.

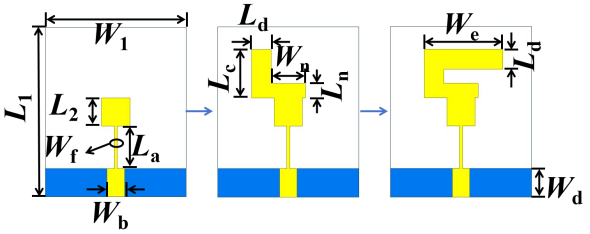

FIGURE 1. The design process of antenna radiation patch.

By optimizing parameter W_e, the antenna's operating bandwidth covers the n261 frequency band. The variation curve of S_{11} with respect to W_e is shown in Fig. 3. The maximum gain measured within the operating frequency band is 3.4 dBi.

2.2. Decoupling Design of the Four-Port MIMO Antenna

In modern communication systems, multi-antenna systems are commonly used to enhance communication capabilities. This is because multi-port antennas can analyze individual components for multipath propagation, as shown in Fig. 4.

The design process of the antenna is shown in Fig. 5. The units of the four-port MIMO antenna are arranged at a 90° angle to each other. The isolation between antenna elements is an important indicator. To reduce the coupling between elements and meet the miniaturization requirements of the antenna, adjacent antenna elements are printed on both sides of the substrate without adding complex decoupling structures.

The separated ground and orthogonally placed antenna elements suppress near-field coupling between adjacent antenna elements. The unit spacing at this point is 5 mm, which is smaller than half of the wavelength $\lambda_{28\,\text{GHz}}/2 = 5.36$ mm, indicating that this method has a decoupling effect. The variations of S_{11}, S_{21}, and S_{31} with structure changes are shown in Fig. 6. It can be observed that the isolation between antenna elements is effectively improved after adopting the above measures. The current distribution at the operating frequency is shown in Fig. 7. The antenna parameters are shown in Table 1.

TABLE 1. Antenna parameter table.

Parameter	Value/mm	Parameter	Value/mm
L_1	6	W_a	0.1
W_1	5	L_b	15
H	0.254	W_b	0.62
L_2	1	L_c	1.7
W_2	1	W_f	0.1
L_3	0.5	L_d	0.7
W_3	1.2	W_d	1
L_a	1.5	W_e	2.78
L_n	0.5	W_n	1.2

3. THEORETICAL ANALYSIS OF 360° RADIATION COVERAGE

The physical antenna is shown in Fig. 8. This four-port MIMO antenna consists of four patch antenna units arranged perpendicular to each other, forming a 90° spatial angle distribution.

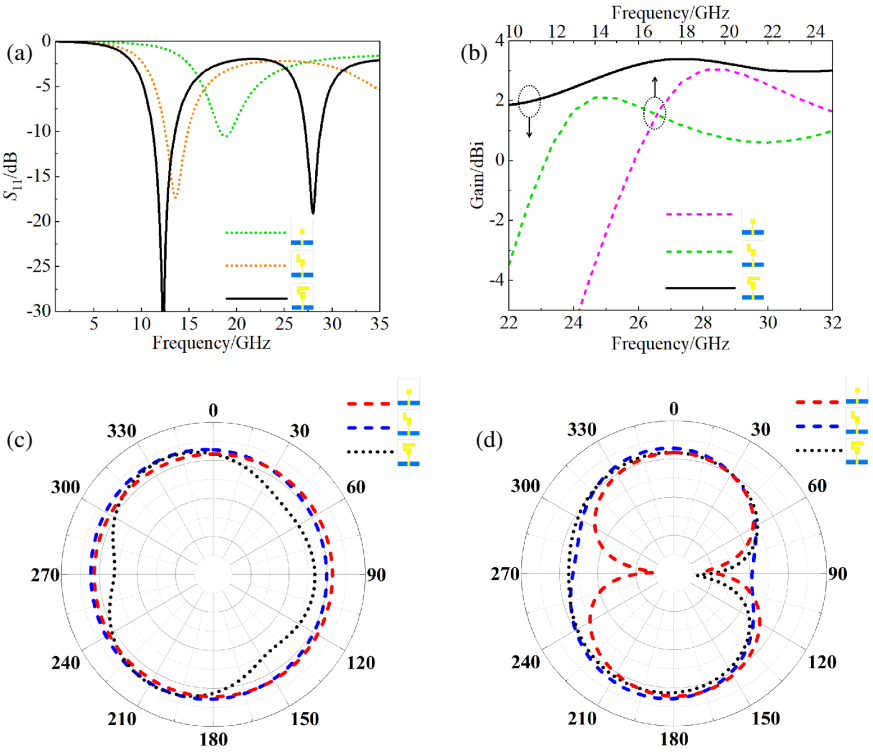

FIGURE 2. With the structure change of (a) S_{11}, (b) gain, (c), (d) radiation pattern.

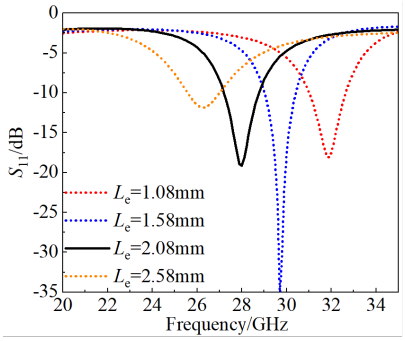

FIGURE 3. Simulation diagram of S_{11} changing with L_e.

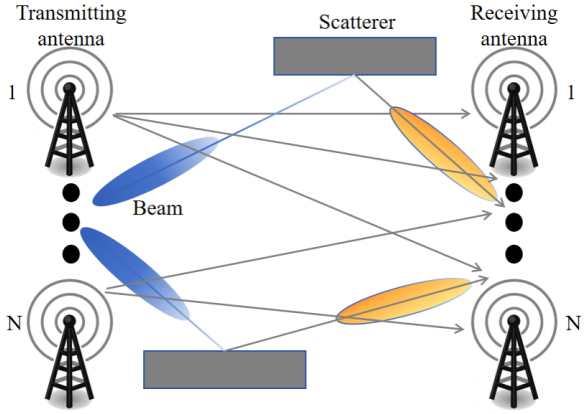

FIGURE 4. Multipath propagation of antennas.

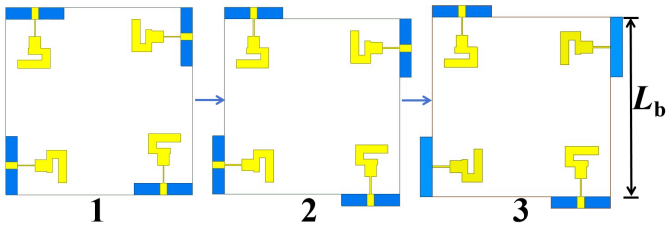

FIGURE 5. Four-port MIMO antenna design process.

Each unit is oriented towards one of the four orthogonal directions in space, as shown in Fig. 8. This unique arrangement naturally provides significant spatial and pattern diversity gain.

When the four-element structure is rotated 90° around its central axis to form the 2 × 4 MIMO antenna shown in Fig. 9, the spatial coordinates of each element and its radiation pattern direction in the global coordinate system also rotate. This geometric transformation alters the relative positioning between elements and shifts the coverage area of each element. In the original orthogonal layout, adjacent antennas experience polarization mismatch, such as port-1 and port-2. Rotating 90° around the central axis results in parallel, opposite-facing adjacent antennas, such as port-1 and port-6. While this increases the coupling between elements, it further enhances the antenna's pattern diversity in both azimuth and elevation angles, allowing the combined beam to cover a broader spatial solid-angle range.

This enhanced spatial diversity characteristic is crucial for overcoming multipath propagation loss caused by obstacles such as buildings in urban vehicular communication environments. The receiver can effectively combine signals from different directions to improve link reliability. For vehicular MIMO antennas, in addition to low mutual coupling and pattern diversity, wide-area coverage capability is equally important. A multi-port MIMO antenna composed of multiple such

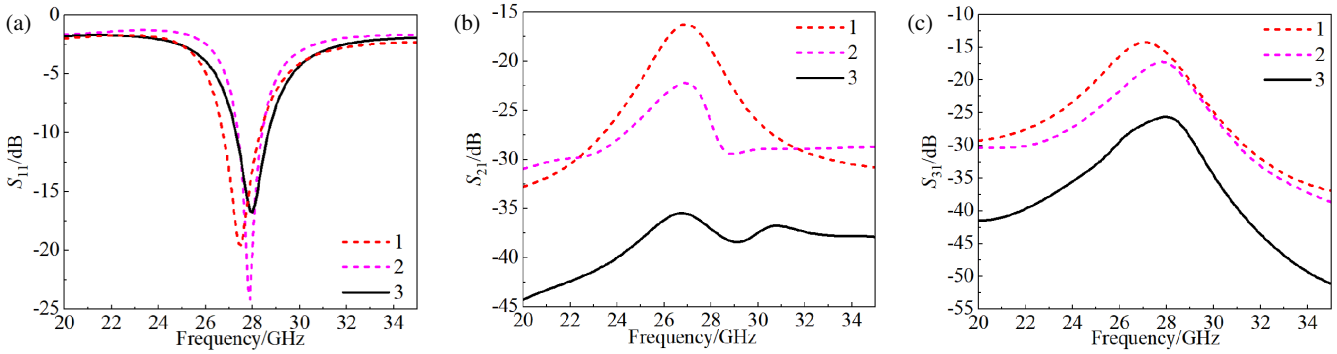

FIGURE 6. S-parameter variation with structure. (a) S_{11}. (b) S_{21}. (c) S_{31}.

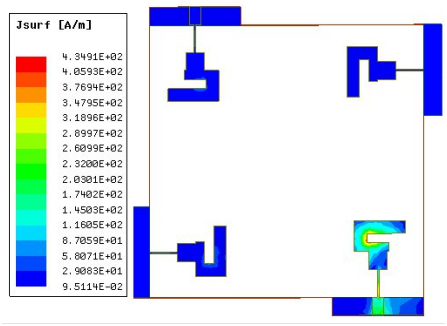

FIGURE 7. Current profile.

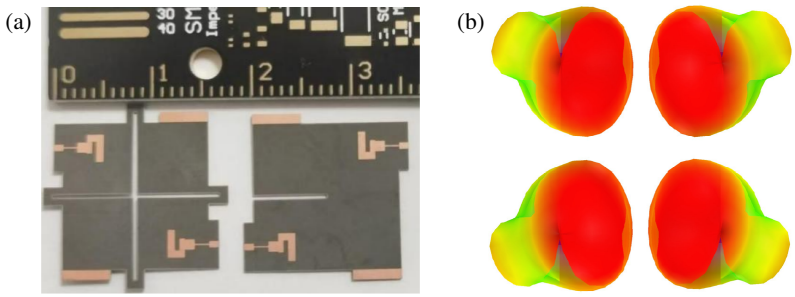

FIGURE 8. 2 × 4 MIMO antenna. (a) Physical. (b) 3D radiation pattern.

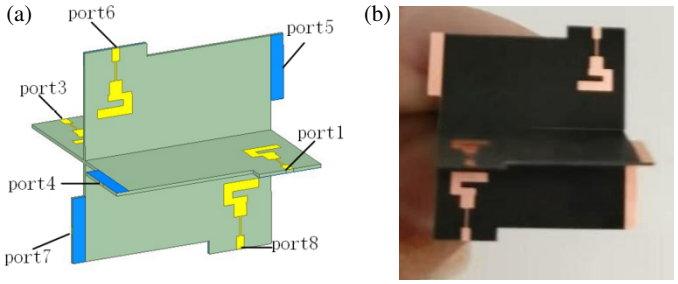

FIGURE 9. 2 × 4 MIMO antenna.

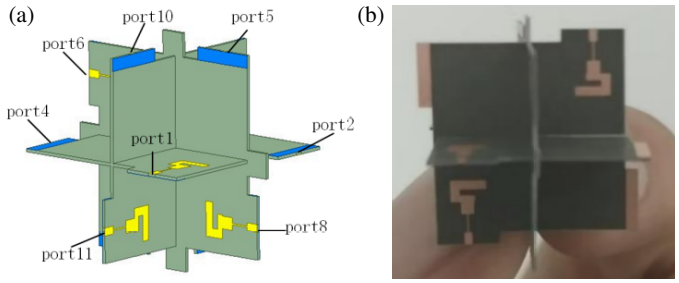

FIGURE 10. 3 × 4 MIMO antenna.

units can achieve full spatial coverage. Fig. 10 shows a 3 × 4 MIMO antenna.

4. ANALYSIS OF SIMULATION AND MEASURED RESULTS

4.1. S-Parameter Analysis

S-parameters are one of the important indicators reflecting the antenna's performance. The simulated and measured reflection coefficients S_{11} for the 2 × 4 MIMO antenna and 3 × 4 MIMO antenna are shown in Fig. 11. From the figure, it can be seen that the operating frequency range of the 3×4 MIMO antenna is 27.28–28.67 GHz, which fully covers the n261 band. Considering the symmetry of the antenna structure, the antenna ports with geometrically symmetric positions have the same isolation. The simulated and measured isolations between some ports are shown in Figs. 12 and 13. Due to the rotation, the relative positions of some antennas become oppositely parallel, with polarization directions matching. Compared to antennas that are vertically oriented in space, the mutual coupling becomes stronger, as seen in S_{61} in Fig. 12 and $S_{11\,8}$ in Fig. 13. However, the isolation is still greater than 18 dB, and the isolation between other ports is greater than 20 dB, meeting the antenna design requirements. It indicates that the antenna in this paper exhibits good isolation characteristics within the operating frequency range.

4.2. Radiation Characteristics

The antenna radiation pattern is one of the important indicators for measuring antenna performance. We measured the radiation pattern of the 3 × 4 MIMO antenna in a microwave anechoic chamber shown in Fig. 14, and the measured radiation patterns of the ports are shown in Fig. 15. The antenna element structure is identical, with each antenna element radiating in

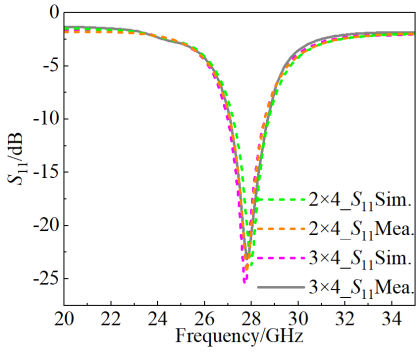

FIGURE 11. S_{11} simulation and measurement results.

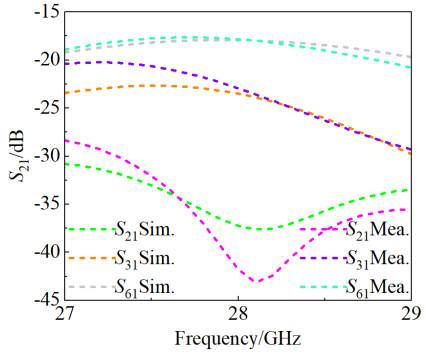

FIGURE 12. 2 × 4 MIMO antenna isolation.

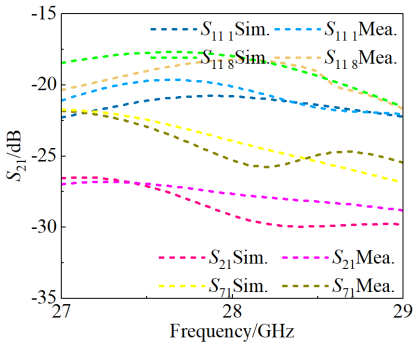

FIGURE 13. 3 × 4 MIMO antenna isolation.

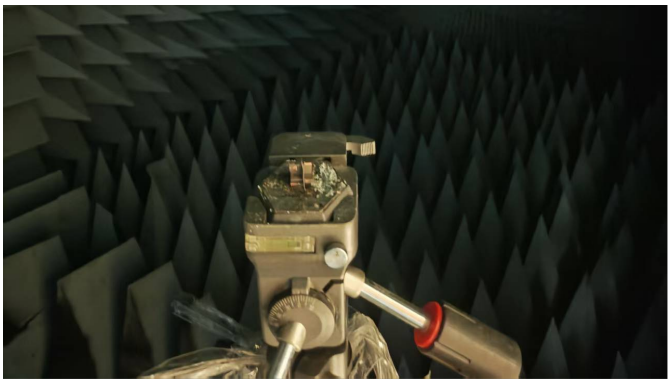

FIGURE 14. Microwave anechoic chamber test environment.

different directions and exhibiting good directivity. In the E-plane radiation pattern, the main beam of port 1 is directed at 0°; the antenna of port 2 radiates at 270°; and the main beams of ports 3 and 4 are directed at 180° and 90°, respectively. The other ports present coverage in specific angular directions. The antenna provides 360° coverage in both the azimuth and elevation planes, and the radiation pattern is diverse, enabling radiation propagation in different planes. It reduces signal multipath propagation loss and enhances communication quality and reliability. The gain of the antenna is shown in Fig. 16.

4.3. Envelope Correlation Coefficient and Diversity Gain

The envelope correlation coefficient (ECC) and diversity gain (DG) of the antenna are important parameters for measuring the independence and diversity performance between MIMO antenna elements. ECC can be calculated using Equation (3):

$$ECC = \frac{|S_{ii}^* S_{ij} + S_{ji}^* S_{jj}|^2}{(1 - |S_{ii}|^2 - S_{jj}^2)(1 - |S_{jj}|^2 - S_{ij}^2)} \tag{3}$$

In the equation, S_{ii}^* and S_{ii} are complex conjugates of each other; S_{ji}^* and S_{ji} are complex conjugates of each other.

DG can be calculated using Equation (4):

$$DG = 10\sqrt{1 - |ECC|^2} \tag{4}$$

Taking the 3 × 4 MIMO antenna as an example, the measured ECC and DG of the antenna are shown in Fig. 17. As can be seen from the figure, the ECC value of the antennas placed face-to-face is higher than that of the antennas placed diagonally. The antenna has an ECC of less than 0.012 and a DG approaching 10 dB within the operating frequency band, indicating that the antenna in this paper exhibits strong signal reception independence and good diversity performance.

4.4. Channel Capacity Loss and Total Active Reflection Coefficient and Mean Effective Gain

Channel capacity loss is a key parameter for calculating the channel loss of highly correlated MIMO antenna systems, and it defines the maximum limit that the information transmission rate can achieve. It is calculated using Equation (5):

$$C_{loss} = -\log_2 \det(\varphi^R) \tag{5}$$

In the equation, φ^R is the correlation coefficient matrix, which can be calculated using Equation (6):

$$\varphi^R = \begin{bmatrix} \rho_{11} & \cdots & \rho_{112} \\ \vdots & \ddots & \vdots \\ \rho_{121} & \cdots & \rho_{1212} \end{bmatrix} \tag{6}$$

ρ_{ij} is calculated using Equations (7) and (8):

$$\rho_{ij} = 1 - \left(\sum_{j=1}^{12} |S_{ij}|^2 \right) \tag{7}$$

$$\rho_{ij} = -(S_{ii}^* S_{ij} + S_{ji}^* S_{jj}) \tag{8}$$

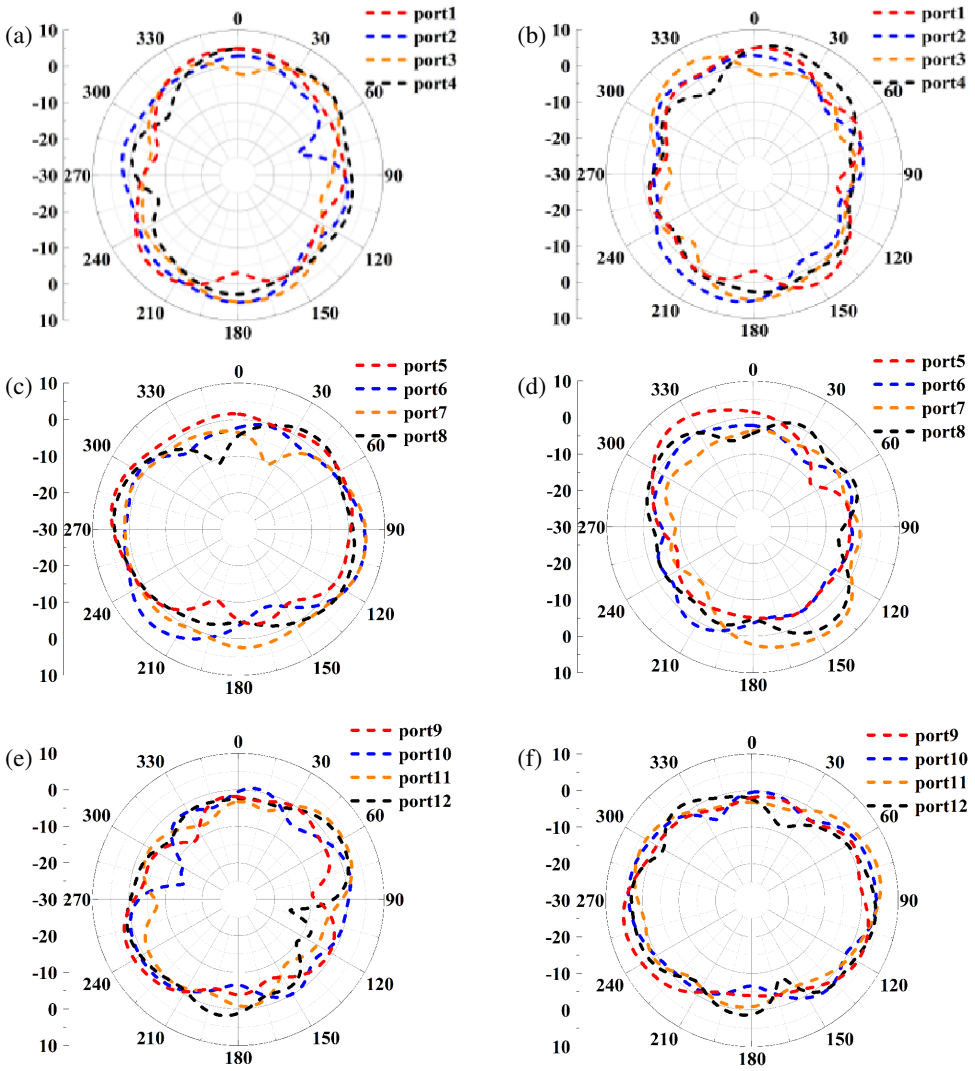

FIGURE 15. Measured radiation patterns of the antenna. (a), (c), (e) E-plane. (b), (d), (f) H-plane.

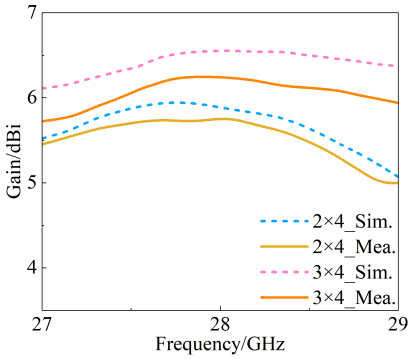

FIGURE 16. Gain of antenna.

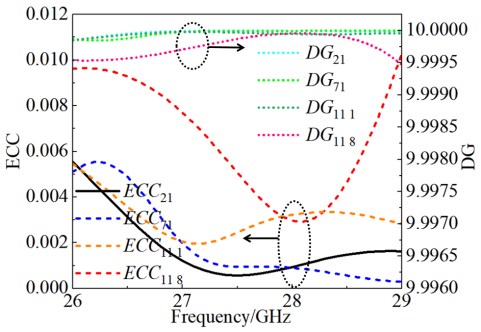

FIGURE 17. The ECC and DG of the antenna.

Figure 18 shows the channel capacity loss (CCL) results for a 3×4 MIMO system. It can be seen that the CCL is below 0.4 bit/s/Hz within the operating frequency band, indicating good data transmission rate.

The total active reflection coefficient is a performance metric that describes the overall performance of a MIMO antenna. It is the ratio of the square root of the total reflected power to the square root of the total incident power. The total active reflection coefficient (TARC) for a 12-port MIMO antenna can be expressed as in Equation (9):

$$TARC = \frac{\sqrt{\sum_{m=1}^{12} |(\sum_{n=1}^{12} S_{mn} e^{j\theta_{mn}})|^2}}{\sqrt{12}} \tag{9}$$

For MIMO antennas, a TARC value less than 0 dB is typically considered the standard. Since θ represents a random

TABLE 2. Antenna performance comparison.

Reference	Number of ports	3D size/mm^3	Bandwidth/GHz	Gain/dBi	Isolation/dB	ECC	360° coverage
[9]	7	$51.7 \times 51.7 \times 51.7$	5.75–5.96	5	> 16.5	< 0.025	No
[10]	8	$128 \times 128 \times 0.76$	9.94–10.09	3.7	> 20	< 0.05	No
[11]	4	$55.2 \times 55.2 \times 1.28$	5.35–5.7	6.4	> 20	< 0.0003	No
[12]	8	$44.4 \times 44.4 \times 1.4$	24–30	7.3	> 24	-	No
[13]	4	$65 \times 25 \times 21$	4.7–5.1	4.1	> 27	-	No
[14]	3	$46 \times 35 \times 3$	5.66–5.94	7.03	> 17.2	< 0.02	No
This work	4	$16 \times 16 \times 0.254$	27.1–28.7	4.39	> 25	< 0.012(12-port)	No
	8	$16 \times 16 \times 16$	27.2–28.58	5.78	> 18		No
	12	$16 \times 16 \times 17$	27.28–28.67	6.25	> 18		Yes

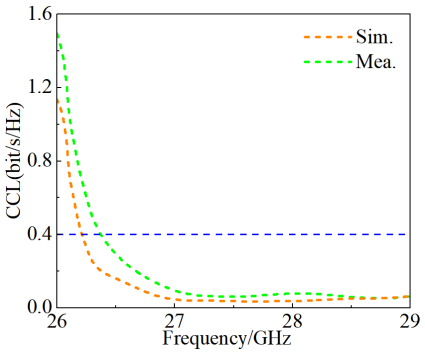

FIGURE 18. The channel capacity loss of the antenna.

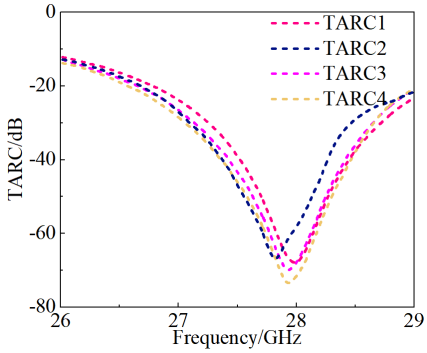

FIGURE 19. The total active reflection coefficient of the antenna.

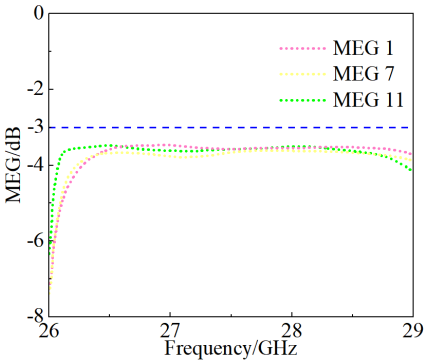

FIGURE 20. The mean effective gain of the antenna.

phase, four sets of phase values were randomly selected from $[0, \pi]$, and the calculation results are shown in Fig. 19. As can be seen in the figure, the four curves converge, and all curve values are below 0 dB within the operating frequency band, confirming the excellent performance of the antenna.

Mean effective gain (MEG) is an important parameter for measuring the diversity performance of MIMO antennas. It can be used to assess the ability of antenna elements to receive electromagnetic signals in multipath fading environments. The MEG measurement results are shown in Fig. 20. As can be seen, MEG 1, MEG 7, and MEG 11 are close to -3 dB within the operating frequency band, with the difference between them maintained within ± 3 dB, meeting the design requirements of the MIMO antenna.

5. PERFORMANCE COMPARISON

The performance comparison of the multi-port MIMO antenna proposed in this paper with other MIMO antennas is shown in Table 2. This paper achieves a good balance between antenna parameters while ensuring antenna performance. It can be seen that compared to antennas in other literature, such as those in [11] and [14], the antenna proposed in this paper has some deficiency in gain. Compared to low-profile antennas, it has some size limitations, but it remains under 2 cm. However, the antenna in this paper does not use complex decoupling methods, allowing the isolation of the multi-port MIMO antenna to remain greater than 18 dB, and 360° beam coverage is achieved through a simple physical structure.

6. CONCLUSION

This paper proposes a millimeter-wave multi-port MIMO antenna design with 360° radiation coverage. The minimum unit consists of a radiation patch, feed line, and ground plane. The antenna units are orthogonally arranged, with adjacent units printed on both sides of the substrate to reduce the coupling between antenna units. The 3D size of the multi-port MIMO antenna is $16 \times 16 \times 17$ mm^3, and it operates in the n261 frequency band. In the 3×4 MIMO antenna, each port exhibits different radiation directions, providing 360° coverage in both azimuth and elevation angles, which meets the requirements of millimeter-wave MIMO antennas for vehicular communication. This design can also be applied to base station antenna deployments, forming narrower and more precise directional beams to enhance terminal reception capability.

ACKNOWLEDGEMENT

I would like to thank the National Natural Science Foundation of China (61971210), my supervisor, Prof. Nan Jingchang, and Liaoning Key Laboratory of Radio Frequency and Big Data for Intelligent Applications for providing the necessary financial support for my research.

REFERENCES

[1] Shariff, B. G. P., T. Ali, P. Kumar, S. Pathan, G. D. G. Simha, P. R. Mane, M. G. N. Alsath, and A.-A. A. Boulogeorgos, "Dual-band compact six-element millimeter wave mimo antenna: Design, characterization, and its application for v2v communication," *IEEE Access*, Vol. 12, 97 951–97 968, 2024.

[2] Tariq, S., S. I. Naqvi, N. Hussain, and Y. Amin, "A metasurface-based MIMO antenna for 5G millimeter-wave applications," *IEEE Access*, Vol. 9, 51 805–51 817, 2021.

[3] Mallat, N. K., M. Ishtiaq, A. U. Rehman, and A. Iqbal, "Millimeter-wave in the face of 5G communication potential applications," *IETE Journal of Research*, Vol. 68, No. 4, 2522–2530, 2022.

[4] Rappaport, T. S., S. Sun, R. Mayzus, H. Zhao, Y. Azar, K. Wang, G. N. Wong, J. K. Schulz, M. Samimi, and F. Gutierrez, "Millimeter wave mobile communications for 5G cellular: It will work!" *IEEE Access*, Vol. 1, 335–349, 2013.

[5] Pi, Z. and F. Khan, "An introduction to millimeter-wave mobile broadband systems," *IEEE Communications Magazine*, Vol. 49, No. 6, 101–107, 2011.

[6] Elfergani, I., A. S. Hussaini, J. Rodriguez, and R. Abd-Alhameed, *Antenna Fundamentals for Legacy Mobile Applications and Beyond*, 1st ed., Springer, Cham, 2017.

[7] Charitos, M. and G. Kalivas, "MIMO HetNet IEEE 802.11p-LTE deployment in a vehicular urban environment," *Vehicular Communications*, Vol. 9, 222–232, 2017.

[8] Karabulut, M. A., A. F. M. S. Shah, and H. Ilhan, "A novel MIMO-OFDM based MAC protocol for VANETs," *IEEE Transactions on Intelligent Transportation Systems*, Vol. 23, No. 11, 20 255–20 267, 2022.

[9] Liu, G.-Y., K. W. Leung, and N. Yang, "Compact radiation-pattern-decoupled MIMO antenna with different radiation directions," *IEEE Transactions on Antennas and Propagation*, 1–1, 2025.

[10] Li, Y. C., K. L. Chu, T. Zhang, and Q. Xue, "A scalable filtering MIMO antenna with space diversity based on shared SIW cavities," *IEEE Antennas and Wireless Propagation Letters*, Vol. 24, No. 7, 1769–1773, Jul. 2025.

[11] Li, R., C. Zhang, and Y. Shao, "A MIMO five-port antenna with pattern and polarization diversity for 5G WLAN applications," in *2025 IEEE International Workshop on Radio Frequency and Antenna Technologies (iWRF&AT)*, 202–204, Shenzhen, China, 2025.

[12] Nuss, B., L. Hampel, and T. Zwick, "Compact broadband 27 GHz aperture-coupled stacked patch MIMO antenna array," in *2025 16th German Microwave Conference (GeMiC)*, 9–12, Dresden, Germany, 2025.

[13] Wang, H., Q. Zheng, Q. Li, and X.-X. Yang, "Isolation improvement and bandwidth enhancement of dual-band MIMO antenna based on metamaterial wall," *IEEE Antennas and Wireless Propagation Letters*, Vol. 24, No. 5, 1144–1148, May 2025.

[14] Chai, B.-T., X. Geng, L. Guo, W. Qin, W.-W. Yang, and J.-X. Chen, "A dual-band tri-port MIMO antenna based on structure reconfiguration," *IEEE Antennas and Wireless Propagation Letters*, 1–5, 2025.

[15] Ullah, H. and F. A. Tahir, "A novel snowflake fractal antenna for dual-beam applications in 28 GHz band," *IEEE Access*, Vol. 8, 19 873–19 879, 2020.

[16] Khan, J., S. Ullah, U. Ali, F. A. Tahir, I. Peter, and L. Matekovits, "Design of a millimeter-wave MIMO antenna array for 5G communication terminals," *Sensors*, Vol. 22, No. 7, 2768, 2022.

[17] Elfergani, I., J. Rodriguez, A. Iqbal, M. Sajedin, C. Zebiri, and R. A. AbdAlhameed, "Compact millimeter-wave MIMO antenna for 5G applications," in *2020 14th European Conference on Antennas and Propagation (EuCAP)*, 1–5, Copenhagen, Denmark, 2020.

[18] Khan, M. I., S. Khan, S. H. Kiani, N. O. Parchin, K. Mahmood, U. Rafique, and M. M. Qadir, "A compact mmWave MIMO antenna for future wireless networks," *Electronics*, Vol. 11, No. 15, 2450, 2022.

[19] Sehrai, D. A., M. Abdullah, A. Altaf, S. H. Kiani, F. Muhammad, M. Tufail, M. Irfan, A. Glowacz, and S. Rahman, "A novel high gain wideband MIMO antenna for 5G millimeter wave applications," *Electronics*, Vol. 9, No. 6, 1031, 2020.

[20] Hussain, N., M.-J. Jeong, A. Abbas, T.-J. Kim, and N. Kim, "A metasurface-based low-profile wideband circularly polarized patch antenna for 5G millimeter-wave systems," *IEEE Access*, Vol. 8, 22 127–22 135, 2020.

[21] Ikram, M., K. S. Sultan, A. M. Abbosh, and N. Nguyen-Trong, "Sub-6 GHz and mm-Wave 5G vehicle-to-everything (5G-V2X) MIMO antenna array," *IEEE Access*, Vol. 10, 49 688–49 695, 2022.

[22] Islam, T., F. N. Alsunaydih, F. Alsaleem, and K. Alhassoon, "Analyzing the performance of millimeter wave MIMO antenna under different orientation of unit element," *Micromachines*, Vol. 14, No. 11, 1975, 2023.

[23] Munir, M. E., S. H. Kiani, H. S. Savci, M. Marey, J. Khan, H. Mostafa, and N. O. Parchin, "A four element mm-wave MIMO antenna system with wide-band and high isolation characteristics for 5G applications," *Micromachines*, Vol. 14, No. 4, 776, 2023.

[24] Sehrai, D. A., M. E. Munir, S. H. Kiani, N. Shoaib, A. D. Algarni, H. Elmannai, M. M. Nasralla, and T. Ali, "A high gain array based millimeter wave MIMO antenna with improved isolation and decorrelated fields," *IEEE Access*, Vol. 12, 89 794–89 803, 2024.